ACS OMEGA

Open Access



http://pubs.acs.org/journal/acsodf

Article

# Template Role of Long Alkyl-Chain Amides in the Synthesis of Zeolitic Imidazolate Frameworks

Kaifei Mu,[#] Jiang Wang,[#] Meizhen Gao, Yanjun Wu, Qi Shi,[*] and Jinxiang Dong

Cite This: *ACS Omega* 2024, 9, 34777−34786

Read Online

ACCESS | Metrics & More | Article Recommendations | Supporting Information

**ABSTRACT:** Organic amides as solvents and structure directing agents (SDAs) are crucial for synthesizing zeolitic imidazolate frameworks (ZIFs). However, current research focuses only on the use of short alkyl-chain amides as solvents/SDAs. Here, we investigate the role of amides with varying alkyl-chain lengths on the structures and topologies of $Zn(Im)_2$ polymorphs. Using short alkyl-chain amides as solvents, the $Zn(Im)_2$ topological structures are affected by the synthesis conditions, leading to "one SDA/multiple topological structures". In contrast, when long alkyl-chain amides are used as solvents, the $Zn(Im)_2$ topological structures are essentially unaffected by other synthesis conditions. Thus, long alkyl-chain amides are shown for the first time to exhibit a significant template role, leading to "one template/one topological structure". Specifically, the use of long alkyl-chain *N*,*N*-dimethyl-C*n* amides (abbreviated as DM-C*n* amides, $n$ = 3, 4, 6, 8, and 10) can lead to only DTF-type $Zn(Im)_2$ frameworks under broad crystallization conditions. Single-crystal X-ray diffraction confirmed that the exquisite structural compatibility between long alkyl-chain DM-C*n* amides and the DFT-type $Zn(Im)_2$ framework results in a highly regular head-to-tail arrangement of amides along the $(kaa\text{-}lov)_n$ chain of the DFT framework. The template role for long alkyl-chain amides was further identified to be multiple C−H···$\pi$ interactions between DM-C*n* amides and $Zn(Im)_2$ frameworks thanks to molecular simulations.

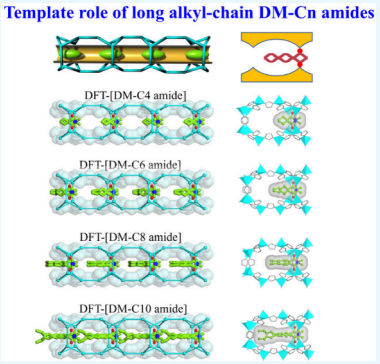


## 1. INTRODUCTION

In the synthetic chemistry of zeolites, structure-directing agents (SDAs) or templates play an essential role in zeolite formation and structural diversity.[1−4] More than 270 types of zeolite skeletal topologies have hitherto been designed and developed.[5] The interesting experimental phenomena of "one template/one topological structure" and "one SDA/multiple topological structures" have long been a focus in zeolite synthesis.[6−9] "One template/one topological structurs" refers to the concept that a specific zeolite structure can only be formed using a specific organic solvent.[2] In this case, the geometry and electronic configuration of the organic molecules and the zeolite framework perfectly match each other. "One SDA/multiple topological structures" means that a given organic solvent can guide the generation of different zeolite structures under various crystallization conditions.[10] These observations support the design of other porous materials with zeolite topologies.[11,12]

Zeolitic imidazolate frameworks (ZIFs), a typical class of porous metal−organic frameworks (MOFs) with zeolite topology, are formed by the self-assembly of tetrahedral metal centers and imidazole-type ligands mimicking the Si−O−Si coordination in zeolites.[13,14] ZIFs generally display superior stability and easily modifiable structures compared to zeolites and MOFs.[15] In ZIF synthesis, the imidazole ligand and synthetic solvent are two equally significant factors that affect the topology and pore structure of ZIFs.[16−18] Relying on abundant imidazole derivatives, more than 50 topological structures of ZIFs, including SOD, CHA, ANA, GME, LTA, ACO, dia, ucb, poz, moz, zeb, and lcs, have been prepared.[19−22]

When a ZIF consists solely of imidazolates, the choice of solvent for its synthesis significantly influences its structure. The 17 known types of $Zn(Im)_2$ complexes (Table S2) have been synthesized in solvents such as $H_2O$, organic amides, N-heterocyclic compounds, macrocyclic compounds, and dimethyl sulfoxide (Figure S1).[23−33] Among these solvents, a typical example is that the use of small-molecular *N*,*N*-dimethylformamide (DMF) can lead to the formation of multiple $Zn(Im)_2$ structures with BCT, GIS, MER, and cag topologies.[19] Conversely, the use of large-sized $MeCH_2CH_2$ cavitand as a "shoe-last" template can guide the assembly of highly porous mer-$Zn(Im)_2$ (ZIF-10) and $Zn(Im)_2$ (RHO).[27,28] In addition, various zeolite structures can be obtained by using a small-sized tetramethylammonium cation ($C_4H_{12}N^+$), while only MEI-type zeolites can be obtained by using a large-sized tris-quaternary ammonium cation ($C_{18}H_{36}N_3^{3+}$).[2,34] This strategy of extending the solvent molecular scale to prepare new

Received: May 4, 2024
Revised: July 20, 2024
Accepted: July 25, 2024
Published: August 3, 2024

zeolite-like structures has inspired us to consider whether using long carbon chain amides might lead to the formation of new $Zn(Im)_2$ structures. To the best of our knowledge, only short alkyl-chain amides such as DMF and *N*,*N*-dimethylacetamide (DMA) have hitherto been used as solvents to synthesize $Zn(Im)_2$, and longer alkyl-chain amides have not been studied.[19,25,29,35]

Hence, the objective of this work is to explore and understand the structure-directing and template role of amides with different alkyl chains in $Zn(Im)_2$ assembly from the experimental and molecular simulation perspectives. In this paper, 1) the dependences of $Zn(Im)_2$ topological structures on organic amide, Zn/Im molar ratio, and crystallization temperature were analyzed; 2) the compatibility between amides and ZIF structures, as well as the dominant factors in different templating roles, was elucidated; and 3) a possible self-assembly pathway of DFT-type ZIFs is proposed. This work may pave the way to a new approach for the targeted synthesis of ZIFs.

## 2. EXPERIMENTAL SECTION

**2.1. Materials.** Imidazole (Im, 99.0%) and zinc acetate dihydrate ($Zn(OAc)_2{\cdot}2H_2O$, 98.0%) were purchased from Sigma-Aldrich Chemical Co., Ltd. *N*,*N*-Dimethylformamide (DM-C1 amide, 99.5%) and *N*,*N*-dimethylacetamide (DM-C2 amide, 99.8%) were obtained from Shanghai Aladdin Biochemical Technology Co., Ltd. *N*,*N*-Dimethylpropionamide (DM-C3 amide, 98%), *N*,*N*-diethylformamide (DE-C1 amide, 99%), and *N*,*N*-diethylacetamide (DE-C2 amide, 99%) were obtained from Anhui Zesheng Technology Co., Ltd. *N*,*N*-Dimethyloctanamide (DM-C8 amide) was obtained from Apollo of J&K Scientific Co., Ltd. *N*,*N*-Dimethyldecanamide (DM-C10 amide, 98.0%) and *N*,*N*-diethylpropionamide (DE-C3 amide, 98.0%) were obtained from TCI Development Co., Ltd. *N*,*N*-Dimethylbutyramide (DM-C4 amide, 98%) and *N*,*N*-dimethylhexanamide (DM-C6 amide, 98%) were obtained from Alfa Aesar Co., Ltd. All chemicals were used as received without further purification.

**2.2. Synthesis.** Typically, a solution of Im (1.0/2.0/3.0 mmol, 0.068/0.136/0.204 g) in DM-Cn amides or DE-C*n* amides (2 mL) was added to a 20 mL glass bottle containing a solution of $Zn(OAc)_2{\cdot}2H_2O$ (0.2 mmol, 0.0439 g) in DM-Cn amides or DE-C*n* amides (1 mL). Subsequently, the undisturbed mixture was maintained at a specific temperature (20, 40, or 60 °C) and left to crystallize for 3 days. The obtained white crystalline products were collected by filtration and dried under ambient conditions. Further details of the synthesis process can be found in the Supporting Information.

**2.3. Crystallography.** Single-crystal X-ray diffraction data were collected at different temperatures on an Agilent Xcalibur Eos Gemini diffractometer employing graphite-monochromated Cu K$\alpha$ radiation ($\lambda$ = 1.54178 Å) or a Bruker SMART-1000 diffractometer employing graphite-monochromated Mo K$\alpha$ radiation ($\lambda$ = 0.71073 Å). Reflection intensities were corrected for absorption by the multiscan method. The structures were solved by direct methods using SHELXS-97 and refined on $F^2$ by the full-matrix least-squares method using SHXLEL-97.[36,37] All non-hydrogen atoms were refined anisotropically. The detailed crystallographic data and refinement parameters are listed in Table S1. The CCDC numbers 2327994−2327998 and 2328136−2328139 contain the supplementary crystallographic data for this paper. These data are accessible through the Cambridge Crystallographic Data Centre.

**2.4. Instrumentation.** Powder X-ray diffraction (PXRD) patterns were recorded on an X-ray diffractometer (Rigaku, MiniFlexII) employing Cu K$\alpha$ radiation ($\lambda$ = 1.5418 Å). $^{13}C$ cross-polarization (CP) magic-angle spinning (MAS) NMR spectroscopy was performed on a Bruker Advance III 600 WB spectrometer operating at 151 MHz at a magnetic field of 14.1 T by using a 4 mm double-tuned MAS probe with a spinning speed of 10.5 kHz. IR spectra were recorded from samples in KBr pellets on an FTIR spectrometer (Shimadzu, Prestige-21). Thermogravimetric (TG) measurements were performed under a static air atmosphere on a simultaneous thermal analyzer (Setaram, Labsys Evo) with a heating rate of 5 K $min^{-1}$.

**2.5. Molecular Simulation.** The molecular simulations in this study were conducted using Material Studio 8.0 and Gaussian 09W software. The structural optimization and stability energy calculations on the frameworks were carried out with the Forcite module. Stability energy ($E_S$) was calculated according to the formula $E_S = E_{A+B} - E_A - E_B$, where $E_{A+B}$ is the total energy of the ZIFs containing the guest molecule, $E_A$ is the energy of the ZIFs without the guest molecule, and $E_B$ is the energy of the amide guest molecule.[6,38]

The sorption performances of ZIFs toward amide molecules were simulated using the Sorption module. The nonbonding interactions through which ZIFs adsorb amide molecules include the Lennard-Jones (LJ) van der Waals potential, Coulombic electrostatic potential, and hydrogen bonding. Of these, the widely employed Dreiding force field distribution is predominantly utilized for modeling the LJ van der Waals potential energy.[39,40] Density functional theory was employed to calculate the partial atomic charges of ZIF fragment clusters and amide molecules. The density functional theory calculations were performed using the B3LYP functional combined with the 6-31G(d) basis set as implemented in Gaussian 09W software (charge distributions of adsorbents and adsorbates are illustrated in Figures S23−S38 and Table S5−S20). Each simulation employed periodic boundary conditions, with a truncated radius of 12.8 Å for the LJ potential energy. Long-range electrostatic potential energy was computed by using the Ewald summation method, with a balance step number of $10^5$ and a sampling step number of $10^6$.

## 3. RESULTS AND DISCUSSION

The crystallization process of $Zn(Im)_2$ is influenced by various factors, including temperature, reactant composition, and type of solvents. In previous research, $Zn(Im)_2$ complexes have been assembled using short alkyl-chain amides as solvents. However, the role of utilizing long alkyl-chain amides in the structure of $Zn(Im)_2$ remains unclear, and this is the focus of this work.

In this article, for ease of description, a series of organic amides used in experiments are systematically named as *N*,*N*-dimethyl-C*n* amides (abbreviated as DM-C*n* amides) and *N*,*N*-diethyl-C*n* amides (abbreviated as DE-C*n* amides), where *n* represents the total number of carbon atoms of the carbonyl group connected to the nitrogen atom and the associated alkyl chains. For example, *N*,*N*-dimethylformamide (DMF) may be named the DM-C1 amide, and *N*,*N*-dimethyldecanamide (DMD) may be named the DM-C10 amide.

**3.1. Influence of Amides with Different Alkyl-Chain Lengths on $Zn(Im)_2$ Topology.** The influences of amides



https://doi.org/10.1021/acsomega.4c04259
ACS Omega 2024, 9, 34777−34786

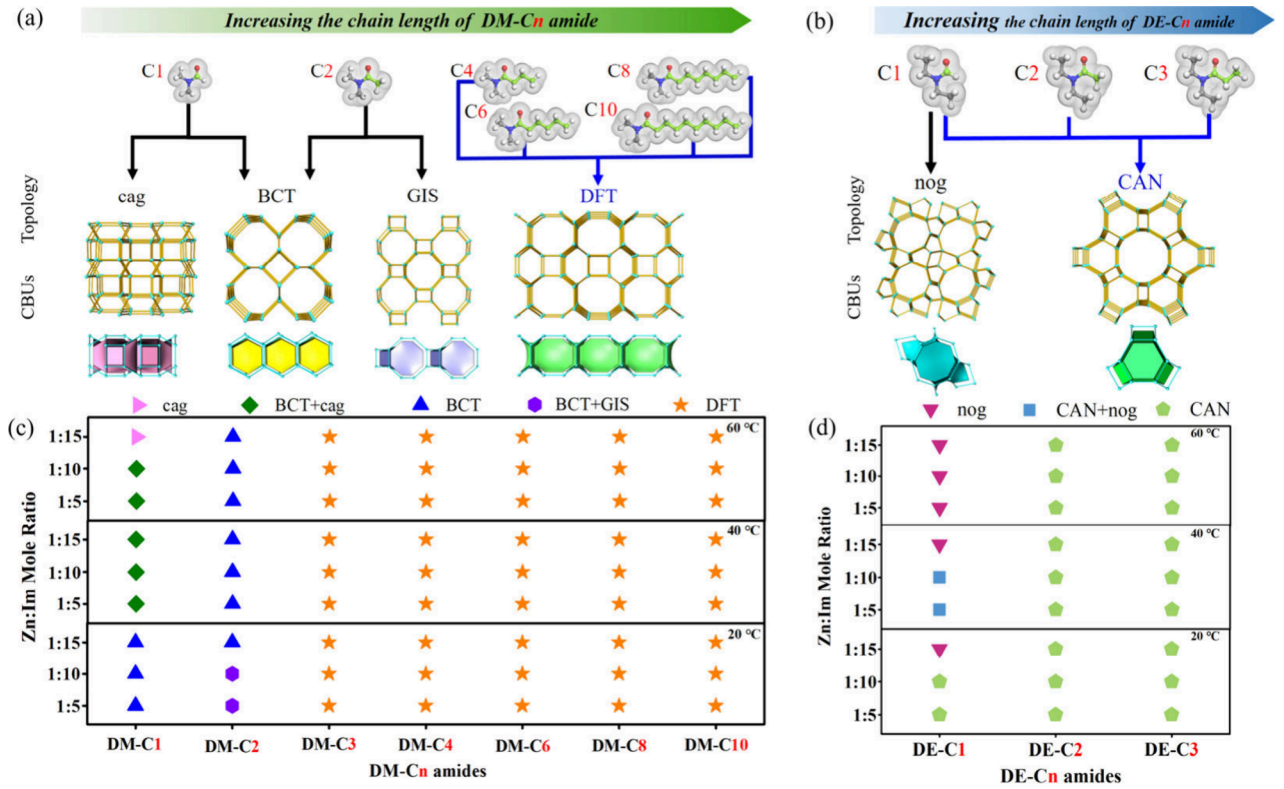


**Figure 1.** Topological structures of $Zn(Im)_2$ generated by (a) DM-C*n* amides and (b) DE-C*n* amides with different alkyl-chain lengths, where CBUs represent the composite building units. (c, d) Influences of DM-C*n* or DE-C*n* amides, Zn/Im molar ratio, and crystallization temperature on $Zn(Im)_2$ topological structures.

with different alkyl-chain lengths, Zn/Im molar ratios, and crystallization temperatures on $Zn(Im)_2$ topological structures were investigated (Figures S2 and S3, Table S3). The crystalline forms of all $Zn(Im)_2$ products were determined through PXRD analysis (Figures S4−S15). As shown in Figure 1c, by using DM-C1 amide as the solvent, BCT-type $Zn(Im)_2$ was successfully crystallized at a low temperature of 20 °C. As the temperature rises to 40 and 60 °C, mixed phases of BCT and cag $Zn(Im)_2$ were obtained. At 60 °C with a Zn/Im molar ratio of 1:15, cag-type $Zn(Im)_2$ was obtained. When crystallized at 80 °C, all $Zn(Im)_2$ products exhibited a cag-type structure, regardless of the Zn/Im molar ratio. When using DM-C2 amide as the solvent, there were some changes in the crystallization results. The more porous GIS-type $Zn(Im)_2$ was formed at a low temperature of 10 °C (Figure S6), whereas at 20 °C, mixed phases of BCT and GIS $Zn(Im)_2$ were formed. As the temperature increases to 40 and 60 °C, pure BCT-type $Zn(Im)_2$ was generated over a wider range of Zn/Im molar ratios, potentially due to solvation differences. Surprisingly, when using longer alkyl-chain DM-C*n* amides (*n* = 3, 4, 6, 8, and 10) as solvents, all $Zn(Im)_2$ products exhibited the DFT topology and were not affected by the given crystallization temperature or Zn/Im molar ratio crystallization conditions.

Furthermore, the use of DE-C*n* amides as solvents in $Zn(Im)_2$ synthesis was also explored (Figure 1d). When DE-C1 amide was used as a solvent, with Zn/Im molar ratios of 1:5 and 1:10, CAN-type $Zn(Im)_2$ was obtained at a low temperature of 20 °C. At the higher temperature of 40 °C with Zn/Im molar ratios of 1:5 and 1:10 mixed phases of CAN- and nog-type $Zn(Im)_2$ were generated. The nog-type $Zn(Im)_2$ tends to form at a high temperature of 60 °C. Surprisingly, when DE-C2 or DE-C3 amide was used as the solvent, only the CAN-type $Zn(Im)_2$ was obtained over a wide range of temperature and Zn/Im molar ratio.

The above experiments indicate that in the crystallization of $Zn(Im)_2$, the structure of the product is highly sensitive to other synthesis factors when using short alkyl-chain amide solvents. When long alkyl-chain amide solvents are used, the structure of $Zn(Im)_2$ is essentially unaffected by other synthesis conditions.

### 3.2. Determination of DM-C*n* and DE-C*n* Amides Included in $Zn(Im)_2$ Frameworks.

$^{13}C$ MAS NMR was conducted to verify the integrity of DM-C*n* and DE-C*n* amides in the obtained $Zn(Im)_2$ frameworks (Figures 2 and 3). The footprints of imidazole ligand in $Zn(Im)_2$ frameworks appear in the range 120−155 ppm (Figures S16 and S17). The peaks of amides can be divided into three regions: the peaks at high chemical shift ($\delta$ = 160.3−192.3 ppm) can be ascribed to the carbonyl carbon; part of the low chemical shift peaks ($\delta$ = 12.1−42.4 ppm) are attributed to alkyl-carbon directly connected to N atoms; and the rest of the alkyl-carbons of the amides collectively contribute to the other low chemical shift peaks. In addition, the gradually widening spectral lines of the alkyl-carbon (from DM-C1 to DM-C10 and DE-C1 to DE-C3 amides) could be due to the changes in various internal nuclear spin interactions caused by enhanced host−guest interaction between $Zn(Im)_2$ and amides.[41]

FT-IR and TG analyses of $Zn(Im)_2$ samples were also conducted to provide supplementary evidence for the inclusion of amides in the corresponding frameworks. The FT-IR spectra of all $Zn(Im)_2$ samples (Figures S18 and S19) exhibited strong carbonyl (C═O) stretching vibration peaks at around 1650 $cm^{-1}$, confirming the presence of amide molecules in the


https://doi.org/10.1021/acsomega.4c04259
ACS Omega 2024, 9, 34777−34786

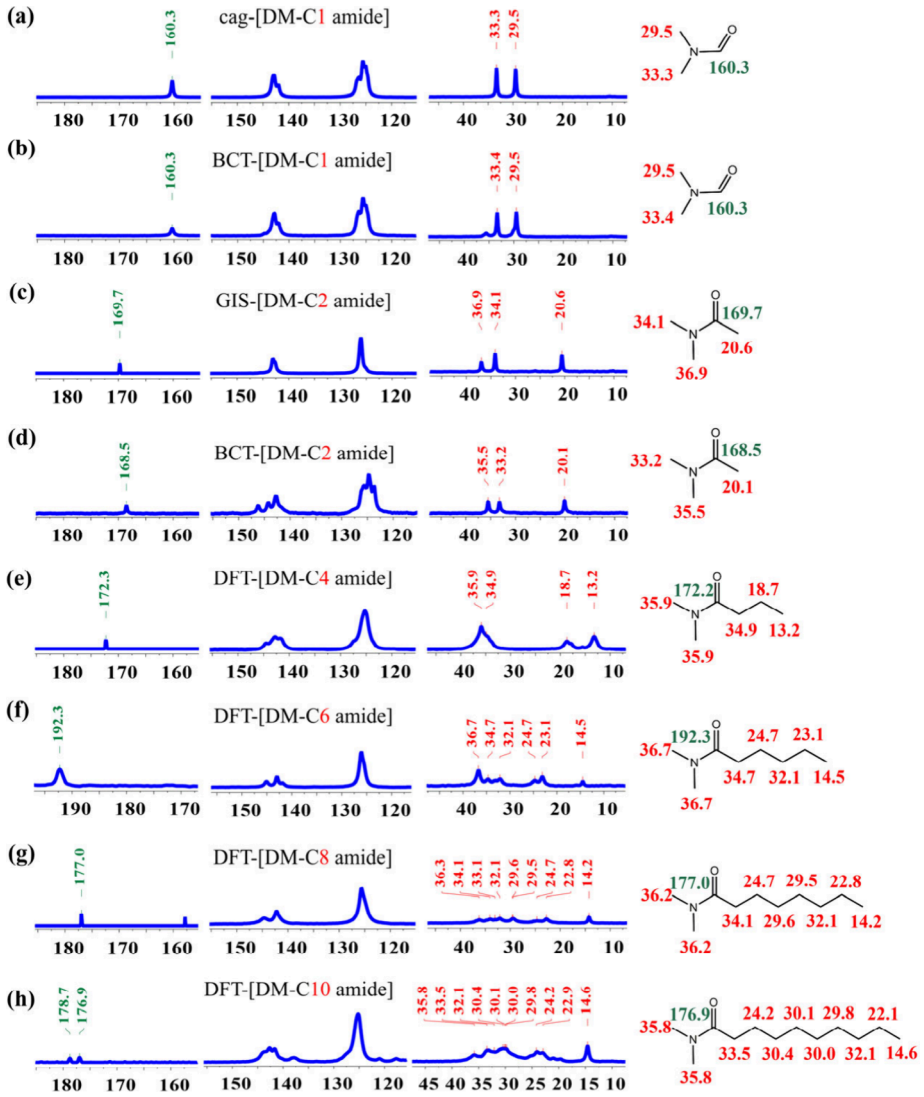


**Figure 2.** $^{13}C$ NMR spectra of $Zn(Im)_2$ samples prepared with (a, b) DM-C1 amide, (c, d) DM-C2 amide, (e) DM-C4 amide, (f) DM-C6 amide, (g) DM-C8 amide, and (h) DM-C10 amide, respectively.

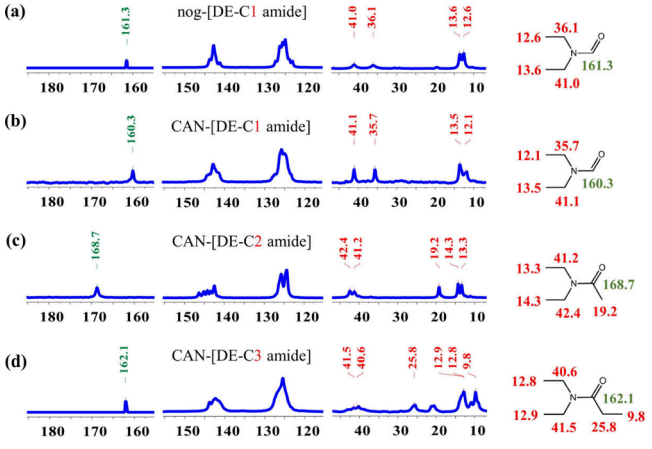


**Figure 3.** $^{13}C$ NMR spectra of $Zn(Im)_2$ samples prepared with (a, b) DE-C1 amide, (c) DE-C2 amide, and (d) DE-C3 amide, respectively.

$Zn(Im)_2$ structure. In addition, the thermal weight loss in the range of 25−300 °C seen in the TG traces (Figures S20 and S21) can be attributed to removal of the amides from the $Zn(Im)_2$ frameworks.

The above observations indicate that DM-C*n* and DE-C*n* amide solvent molecules are included in $Zn(Im)_2$ frameworks. However, the structural compatibility between $Zn(Im)_2$ and amides remains ambiguous. Further exploration is needed to gain a deeper understanding of the structure-directing and template mechanisms of amide solvents in the synthesis of $Zn(Im)_2$ structures.

**3.3. Exquisite Structural Compatibility of "One Template/One $Zn(Im)_2$ Topological Structure".** To determine the localization of amide molecules in $Zn(Im)_2$, single-crystal X-ray diffraction data were collected from the respective polymorphs. For GIS-[DM-C2 amide] and CAN-[DE-C1 amide] samples, for which single-crystal X-ray diffraction data could not be collected, the most probable binding sites within $Zn(Im)_2$ were determined by using the sorption module in Materials Studio 8.0 software. Based on this, a more profound analysis and discussion of the phenomenon of "one template/one topological structure" is elaborated in this section, and "one SDA/multiple topological structures" will be discussed in the following section.



https://doi.org/10.1021/acsomega.4c04259
ACS Omega 2024, 9, 34777−34786

Figure 4 provides an overview of the structural compatibility between DM-C*n* amides and DFT-type frameworks. In Figure 4a, it can be seen that the DFT topology is composed of three basic tiles: *lov* [$4^2.6^2$], *ste* [$4^2.8^4$], and *kaa* [$6^2.8^2$]. The [$4^2.6^2.8^2$] is composed of one *kaa* and one *lov* tile, which is denoted as a *(kaa-lov)* composite building unit (CBU). Furthermore, multiple [$4^2.6^2.8^2$] CBUs are interconnected to form $(kaa\text{-}lov)_n$ chains.

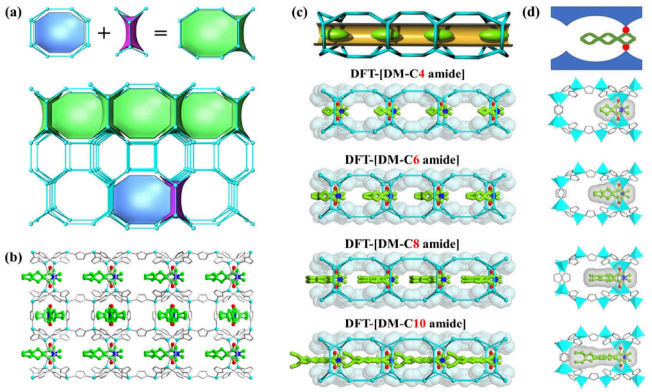


**Figure 4.** (a) Composite building units and chains composed of *kaa* and *lov* tiles in the DFT framework. (b) Typical example of the DM-C6 amide as a template included in the DFT framework. Localization of DM-C*n* amides in the (c) $(kaa\text{-}lov)_n$ channel and in the (d) *(kaa-lov)* composite building units of the DFT framework.

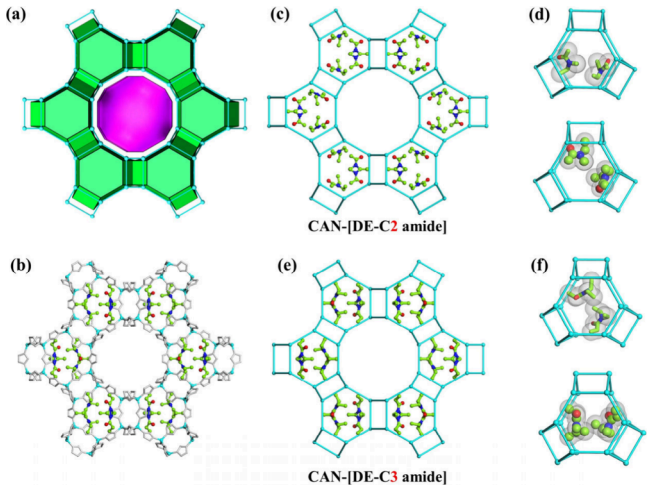


**Figure 5.** (a) The tiles of *can* and *ato* in the CAN framework. (b) Typical example of DE-C2 amide as template included in the CAN framework. (c, d) The localization of DE-C1 amide in the *can* cage of the CAN framework. (e, f) The localization of DE-C2 amide in the *can* cage of the CAN framework.

For a simplified description of the structural compatibility between amides and the DFT framework, for any given DM-C*n* amides, the *N*,*N*-dimethyl segment, carbonyl group segment, and remaining alkyl-chain segment may be considered as the head, shoulder, and tail, respectively. In Figure 4d, single-crystal results reveal that the solvent-accessible surface of the DM-C*n* amides may be a reasonable location for the organic amides within the DTF-type $Zn(Im)_2$. Specifically, the head of each DM-C*n* amide precisely passes through the six-membered ring (6-MR) of *lov*, leaving it parallel to the $(kaa\text{-}lov)_n$ chain channel. The shoulder of each DM-C*n* amide is perpendicular to the 4-membered ring (4-MR) of *lov*, and the tails of the DM-C*n* amides are extend freely along the $(kaa\text{-}lov)_n$ chain (see Figure 4c). Eventually, all DM-C*n* amide molecules can be confined within the pores of the DFT-[DM-C*n*] framework and exhibit a highly consistent orientation in a head-to-tail manner. As the alkyl chains of DM-C*n* amides increase, the cavity volume of the CBUs occupied by amides increases from approximately one-third to complete occupation. These results strongly support the templating role of the amide in the assembly of DFT-type $Zn(Im)_2$ structures.

The distribution of DE-C*n* amide molecules in the CAN topology was also discussed to further understand the phenomenon of "one template/one topological structure". From a topological perspective, the CAN structure is built from *ato* [$6^3.12^2$] tiles, forming 12-membered ring (12-MR) channels parallel to the *a*-axis surrounded by *can* [$4^6.6^5$] tiles, as shown in Figure 5a.

Interestingly, a good geometrical fit was observed between the DE-C*n* amide ($n$ = 2, 3) templates and the *can* cage in CAN-$Zn(Im)_2$. Each *can* cage can capture and accommodate two template molecules. Through careful comparison, it was established that all carbonyl groups (−C═O) of all DE-C*n* amides point approximately toward the intersection, which is shared by two 6-MR and one 4-MR in the *can* cage. In Figure 5d, the two N-ethyl chains of one DE-C2 amide molecule are seen to be parallel to two different 6-MRs, and the C2-alkyl chain is perpendicular to one 6-MR. In another DE-C2 amide, one N-ethyl chain is perpendicular to the 6-MR, while the other N-ethyl chain points toward the intersection of the two 4-MRs, and the C2-alkyl chain is parallel to the 6-MR. In Figure 5f, the configurations of two DE-C3 amides within the same *can* cage are akin to that of the aforementioned DE-C2 amide, albeit with slight variations. A more detailed comparison can be found in Table S22. The adaptive configurations of DE-C*n* amide molecules within the *can* cage suggest that it is logical to consider amides as templates favoring the formation of *can* cages.

**3.4. General Structural Compatibility of "One SDA/Multiple $Zn(Im)_2$ Topological Structures".** Unlike the structural compatibility between long alkyl-chain amide templates and DFT frameworks, the presence of general short alkyl-chain amide SDAs is a necessary but not sufficient condition for the generation of specific $Zn(Im)_2$ structures. As shown in Figure 6, BCT- and cag-type $Zn(Im)_2$ were obtained using DM-C1 amide as solvent, while the BCT- and GIS-type $Zn(Im)_2$ were obtained using DM-C2 amide as solvent. For these short alkyl-chain amides, their corresponding $Zn(Im)_2$ frameworks provide ample space for free movement or rotation of the amides, leading to at least two possible orientations within the $Zn(Im)_2$ cage. In this case, these amides act as SDAs, behaving more like solvents that fill the $Zn(Im)_2$ pores without being tightly bound at specific positions within the $Zn(Im)_2$ framework. Such a phenomenon of "one SDA/multiple $Zn(Im)_2$ structures" originates from the influence of changes in crystallization conditions on the properties of the SDA itself. These changes alter the distribution of the CBU types and the assembly pathway followed during crystallization, ultimately affecting the strength and mode of interaction between SDAs and CBUs.

**3.5. Quantitative Analysis of Structure-Directing and Template Role of Amides on $Zn(Im)_2$ Structures.** Molecular simulation methods were applied to quantify the


https://doi.org/10.1021/acsomega.4c04259
ACS Omega 2024, 9, 34777−34786

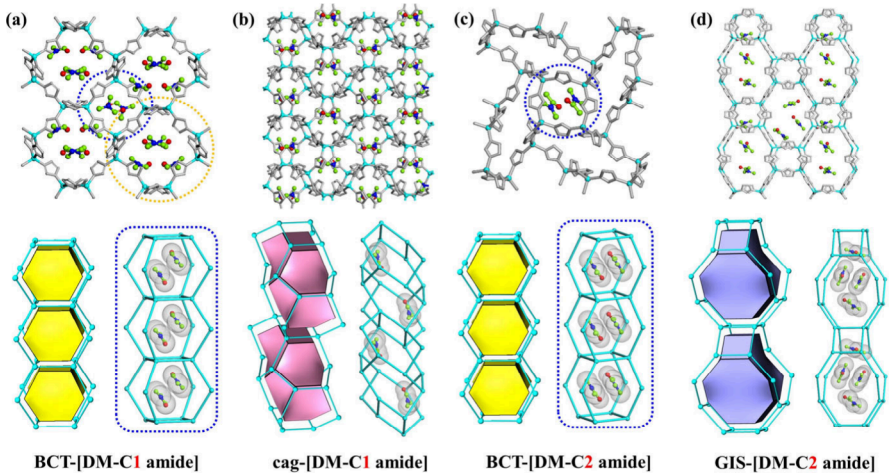


**Figure 6.** General structural compatibility relationship between short alkyl-chain DM-C*n* amides and corresponding $Zn(Im)_2$ frameworks. (a) BCT-[DM-C1 amide], (b) cag-[DM-C1 amide], (c) BCT-[DM-C2 amde], and (d) GIS-[DM-C2 amide].

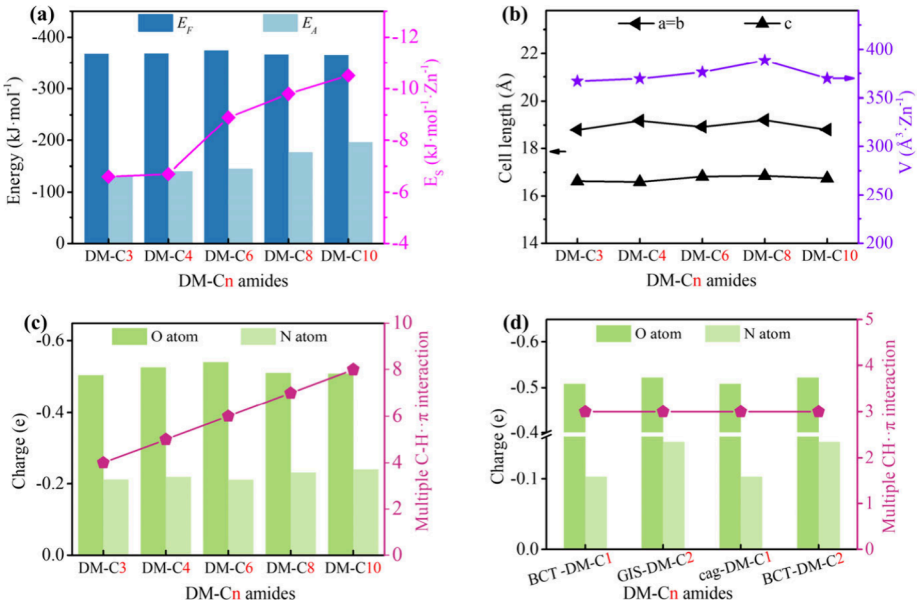


**Figure 7.** Different structure-directing and template abilities of DM-C*n* amides on $Zn(Im)_2$ structures. (a) The long alkyl-chain DM-C*n* amides' energy $E_A$, DFT-$Zn(Im)_2$ frameworks' energy $E_F$, and the host−guest stability energy $E_S$. (b) Cell lengths and cell volumes of DFT-$Zn(Im)_2$ prepared using long alkyl-chain DM-C*n* amides. The charge on the nitrogen and oxygen atoms in (c) long alkyl-chain and (d) short alkyl-chain DM-C*n* amides and their corresponding multiple C−H···$\pi$ interactions between these amides and the $Zn(Im)_2$ frameworks.

different host−guest interactions (related to the distance of host−guest and the amount of charge) between $Zn(Im)_2$ and DM-C*n* amides.[42] According to previous research, open frameworks can be synthesized only through the use of amides, as opposed to alkanes of comparable dimensions. This indicates that the structure-directing role of amides is closely related to those of their nitrogen and oxygen atoms. On this basis, the energy of the $Zn(Im)_2$-hosts and amide-guests, the atomic charges on nitrogen and oxygen in the amides, and the multiple C−H···$\pi$ interactions were analyzed to explore the origins of the differences between the phenomena of "one template/one $Zn(Im)_2$ topological structure" and "one SDA/multiple $Zn(Im)_2$ topological structures".

The strength of a host−guest interaction is reflected by the stability energy ($E_S$), which is calculated as the difference between the host−guest energy ($E_{F\text{-}A}$) and the summation of the frameworks energy ($E_F$) and the amide energy ($E_A$). As can be seen in Figure 7a, the strong template role of long alkyl-chain DM-C*n* amides ($n \geq 3$) triggers the phenomenon of "one template/one topological structure". For the five DFT-[DM-C*n*] $Zn(Im)_2$ ($n$ = 3, 4, 6, 8, and 10), $E_S$ values of −6.6, −6.7, −8.9, −9.8, and −10.5 kJ·mol$^{-1}$·Zn$^{-1}$, respectively, were calculated (the number of tetrahedral centers normalizes this value).

The increasingly negative $E_S$ values indicate that with increasing alkyl chain length in DM-C*n* amides their host−guest binding and templating abilities are enhanced. In addition, all $E_F$ values of the DFT frameworks are very similar, as evidenced by the basically unchanged cell length and volume of the DFT-type $Zn(Im)_2$ polymorphs (see Figure 7b). This suggests that the framework makes a minimal contribution to the variation in $E_S$. The increased $E_A$ values can be attributed to the prolonged alkyl chains in the DM-C*n* amides. Subsequently, the charges on the nitrogen (N) and


https://doi.org/10.1021/acsomega.4c04259
ACS Omega 2024, 9, 34777−34786

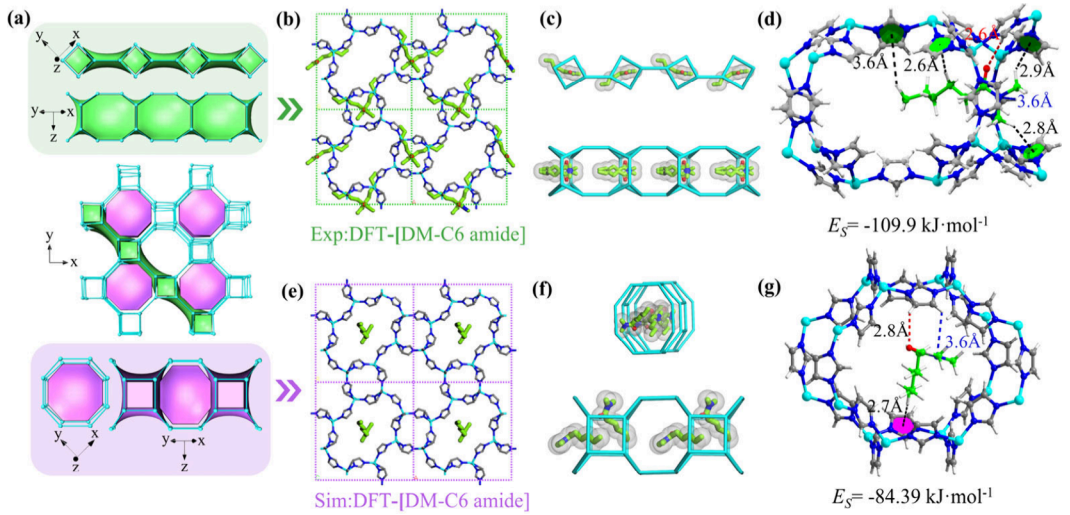


**Figure 8.** (a) Comparison of the DM-C*n* amides filling direction determined through experiment (channel formed by green tiles) and simulation (channel formed by magenta tiles) in the DFT-type framework. The localization of DM-C6 amide in a DFT-type framework and corresponding host−guest interactions based on (b−d) single-crystal results and (e−g) molecular simulation results.

oxygen (O) atoms of all DM-C*n* amides were calculated to remain essentially unchanged (Figure 7c), which excludes any influence on the variation in the structure-directing abilities of the amides. In contrast, the most significant difference that accounts for the increased structure-directing ability of the amides lies in the increased multiple C−H···$\pi$ interactions (Figure S39). In these DM-C*n* amide induced Zn(Im)$_2$ structures, it can be observed that the number of host−guest C−H···$\pi$ interactions increases with the extension of the alkyl chain in amides, and these interaction distances range from 2.5 to 3.7 Å. In addition, the configurations of DM-C*n* amides are not completely straight, but rather curved in some directions, which also implies the important role of multiple C−H···$\pi$ interactions. Therefore, it is reasonable to attribute the strong template role of amides to the multiple C−H···$\pi$ interactions between DM-C*n* amides and the Zn(Im)$_2$ frameworks. In fact, similar results have also been observed in CAN-[DE-C*n* amides] Zn(Im)$_2$ (Figures S40 and S41; Table S24), which further supports our inferences.

As seen in Figure 7d, for multiple Zn(Im)$_2$ structures induced by short alkyl-chain amides (DM-C1 and DM-C2 amides), there are three C−H···$\pi$ interactions between DM-C*n* amides and the corresponding Zn(Im)$_2$ (Table S24). This result is inconsistent with the DFT-[DM-Cn amides] ZIFs synthesized using long alkyl-chain DM-C*n* amides ($n$ = 3, 4, 6, 8, and 10). As regards the atomic charges in DM-C1 and DM-C2 amides, that on their oxygen atoms remains unchanged, whereas that on the nitrogen atoms undergoes a significant change (from −0.103*e* to −0.153*e*). Therefore, it can be concluded that the variation in the weak structure-directing role of short alkyl-chain amides stems from the charge on their nitrogen atoms, which are readily affected by the crystallization environment, consequently diminishing the structure-directing role of amides on Zn(Im)$_2$ structures.

**3.6. The Localization of Amides and Possible Crystallization Pathway in DFT-Type Frameworks.** Molecular simulation was used to predict or examine the optimal adsorption positions of amides in empty Zn(Im)$_2$ frameworks. After loading the relevant adsorbate, the positions of amides in the BCT, cag, nog, and CAN frameworks derived from simulation results showed good consistency with single-crystal XRD analysis results (Figures S42−S44), with only slight differences in loading quantity and adsorption configuration.

However, completely different results from experiment and simulation were observed for the DFT framework (Figure S45). As described in experiments Section 3.2, DM-C6 amide acts as a template within the 6-MR channel, continuously extending in the CBUs of the DFT framework. The DM-C6 amide structure fits perfectly within the Zn(Im)$_2$ structure, making this combination reasonable. The simulation results in Figure 8e suggest that the DM-C6 amide did not appear in the expected channel (formed by green tiles) but appeared in the large channel (formed by magenta tiles). In this channel, the DM-C6 amide is loosely bound to the pore wall with a weaker host−guest interaction. During the simulation process, the binding position of the DM-C6 amide within the DFT-type Zn(Im)$_2$ always remained within the 8-MR channel regardless of the number of loaded amide molecules (Figure S41). This observation may indicate that the amide molecule has difficulty in entering the small channel position after the DFT framework is formed. Therefore, it can be reasonably inferred that the DM-C6 amide may have been incorporated during the formation of *(kaa-lov)* CBUs in Zn(Im)$_2$ and that this was followed by the assembly of ste CBUs. The simulation results of loading one amide molecule on each of these two CBUs show that the stability energy ($E_B$) of DM-C6 amide within *(kaa-lov)* (−109.9 kJ·mol$^{-1}$) is more negative than that within *ste* (−84.39 kJ·mol$^{-1}$), indicating that DM-C6 amide exhibits a stronger template role within the *(kaa-lov)* CBUs.

Based on the above discussion, a possible crystallization pathway for DFT-type Zn(Im)$_2$ is proposed, which is deemed universally applicable for DM-C*n* amides ($n$ > 2) due to their similar structural properties (see Figure 9). First, many relatively tight tiles of *kaa* and *lov* are formed by the assembly of Im ligands and $Zn^{2+}$ around the DM-C*n* amide molecules. Subsequently, these individual *kaa* and *lov* tiles are further alternately assembled with the help of DM-C*n* amides to form *(kaa-lov)* CBUs, which can be further assembled into *(kaa-lov)*$_n$ chains. Finally, these composite units are assembled to form a DFT topology with free amides filling the 8-MR channels.


https://doi.org/10.1021/acsomega.4c04259
ACS Omega 2024, 9, 34777−34786

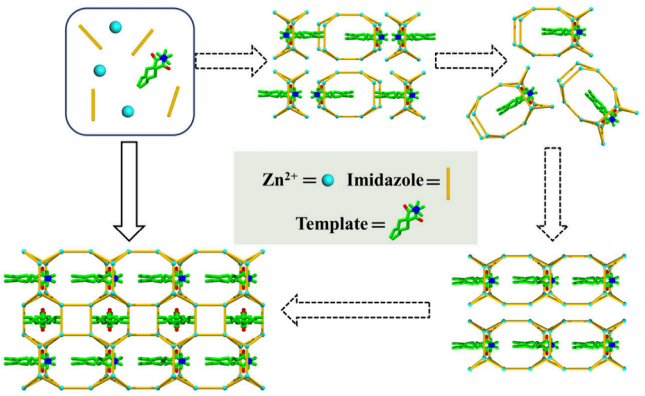


**Figure 9.** Possible crystallization pathway of DFT-type $Zn(Im)_2$ structures.

## 4. CONCLUSION

In summary, the structure-directing and template roles of different amides on $Zn(Im)_2$ topological structures have been systematically studied by using a series of alkyl amides of varying chain lengths as synthetic solvents. When using short alkyl-chain amides as solvents, the topological structure of $Zn(Im)_2$ is affected by the synthesis conditions, and multiple $Zn(Im)_2$ topological structures ware obtained. In contrast, the utilization of long alkyl-chain DM-C*n* amides ($n$ = 3, 4, 6, 8, and 10) can lead only to DTF-type $Zn(Im)_2$ frameworks over a wide range of temperatures and Zn/Im molar ratios. Thus, the extension of alkyl-chain length in amides can significantly strengthen the templating role, leading to an obvious transition from "one short alkyl-chain amide/multiple $Zn(Im)_2$ topological structures" to "one long alkyl-chain amide/one $Zn(Im)_2$ topological structure". Specifically, long alkyl-chain DM-C*n* amides exhibit a highly regular head-to-tail arrangement along the $(kaa\text{-}lov)_n$ chain of the DFT framework, which indicates the exquisite structural compatibility between long alkyl-chain DM-C*n* amides and the DFT-type $Zn(Im)_2$ framework. The observed exquisite structural compatibility between long alkyl-chain DM-C*n* amides and the DFT-$Zn(Im)_2$ structure is primarily attributed to their multiple C−H···$\pi$ interactions. As regards the general structural compatibility between short alkyl-chain amides and multiple $Zn(Im)_2$ structures, their differing directing abilities stem from the variations on the charge of nitrogen atoms. Based on the significant differences between the experimental and simulated DM-C6 amide positions, it can be reasonably inferred that a long alkyl-chain DM-C6 amide as a template leads to the formation of $(kaa\text{-}lov)_n$ chains of the DFT framework. Our work provides unique insights into the role of SDAs and templates in synthesizing $Zn(Im)_2$ polymorphs as well as in the targeted design of crystalline porous materials. A deeper understanding of the crystallization pathway of $Zn(Im)_2$ requires the use of in situ analysis and other methods, which may be the focus of our future research work.

## ■ ASSOCIATED CONTENT

### Supporting Information

The Supporting Information is available free of charge at https://pubs.acs.org/doi/10.1021/acsomega.4c04259.

Crystallographic data and structural information; characterization of PXRD, TG, IR, $^{13}C$ NMR, and 77 K $N_2$ isotherm; molecular simulation information on $Zn(Im)_2$ (PDF)

X-ray crystallographic data (CCDC number 2327994) (CIF)

X-ray crystallographic data (CCDC number 2327995) (CIF)

X-ray crystallographic data (CCDC number 2327996) (CIF)

X-ray crystallographic data (CCDC number 2327997) (CIF)

X-ray crystallographic data (CCDC number 2327998) (CIF)

X-ray crystallographic data (CCDC number 2328136) (CIF)

X-ray crystallographic data (CCDC number 2328137) (CIF)

X-ray crystallographic data (CCDC number 2328138) (CIF)

X-ray crystallographic data (CCDC number 2328139) (CIF)

## ■ AUTHOR INFORMATION

### Corresponding Author

**Qi Shi** − *College of Chemical Engineering and Technology, Shanxi Key Laboratory of Chemical Product Engineering, Taiyuan University of Technology, Taiyuan 030024, People's Republic of China;* orcid.org/0000-0003-0464-6354; Email: shiqi594@163.com

### Authors

**Kaifei Mu** − *College of Chemical Engineering and Technology, Shanxi Key Laboratory of Chemical Product Engineering, Taiyuan University of Technology, Taiyuan 030024, People's Republic of China*

**Jiang Wang** − *College of Chemical Engineering and Technology, Shanxi Key Laboratory of Chemical Product Engineering, Taiyuan University of Technology, Taiyuan 030024, People's Republic of China*

**Meizhen Gao** − *College of Chemical Engineering and Technology, Shanxi Key Laboratory of Chemical Product Engineering, Taiyuan University of Technology, Taiyuan 030024, People's Republic of China*

**Yanjun Wu** − *College of Chemical Engineering and Technology, Shanxi Key Laboratory of Chemical Product Engineering, Taiyuan University of Technology, Taiyuan 030024, People's Republic of China*

**Jinxiang Dong** − *College of Chemical Engineering and Technology, Shanxi Key Laboratory of Chemical Product Engineering, Taiyuan University of Technology, Taiyuan 030024, People's Republic of China;* orcid.org/0000-0001-5623-3514

Complete contact information is available at: https://pubs.acs.org/10.1021/acsomega.4c04259

### Author Contributions

#Kaifei Mu and Jiang Wang contributed equally to this work.

### Notes

The authors declare no competing financial interest.

## ■ ACKNOWLEDGMENTS

This work was supported by the National Natural Science Foundation of China (Nos. 22278289 and 21822808). We

thank International Science Editing for editing this manuscript (http://www.internationalscienceediting.com).

## REFERENCES

(1) Moliner, M.; Rey, F.; Corma, A. Towards the rational design of efficient organic structure-directing agents for zeolite synthesis. *Angew. Chem., Int. Ed.* **2013**, *52*, 13880−9.
(2) Li, J. Y.; Yu, J. H.; Xu, R. R.; et al. The structure directing and templating effects in the formation of microporous compounds. *Chinese Journal of Inorganic Chemistry* **2004**, *20*, 1−16.
(3) Dhainaut, J.; Daou, T. J.; Chappaz, A.; et al. Synthesis of FAU and EMT-type zeolites using structure-directing agents specifically designed by molecular modelling. *Microporous and mesoporous materials* **2013**, *174*, 117−125.
(4) Guo, X.; Geng, S.; Zhuo, M.; et al. The utility of the template effect in metal-organic frameworks. *Coord. Chem. Rev.* **2019**, *391*, 44−68.
(5) Database of Zeolite Structures. Zeolite Framework Types. http://asia.iza-structure.org/IZA-SC/ftc_table.php (accessed on April 23, 2024).
(6) Xin, L.; Sun, H.; Xu, R.; et al. Origin of the structure-directing effect resulting in identical topological open-framework materials. *Sci. Rep.* **2015**, *5*, No. 14940.
(7) Zhao, N.; Cai, K.; He, H. The synthesis of metal-organic frameworks with template strategies. *Dalton Transactions* **2020**, *49*, 11467−11479.
(8) Lu, H. Y.; Yan, Y.; Tong, X. Q.; et al. The structure-directing effect of n-propylamine in the crystallization of open-framework aluminophosphates. *Science China Chemistry* **2014**, *57*, 127−134.
(9) Yan, W.; Song, X.; Xu, R. Molecular engineering of microporous crystals: (I) New insight into the formation process of open-framework aluminophosphates. *Microporous Mesoporous Mater.* **2009**, *123*, 50−62.
(10) Tong, X.; Xu, J.; Li, X.; et al. Molecular engineering of microporous crystals: (VII) The molar ratio dependence of the structure-directing ability of piperazine in the crystallization of four aluminophosphates with open-frameworks. *Microporous Mesoporous Mater.* **2013**, *176*, 112−122.
(11) Zhai, Q. G.; Bu, X.; Mao, C.; et al. An ultra-tunable platform for molecular engineering of high-performance crystalline porous materials. *Nat. Commun.* **2016**, *7*, No. 13645.
(12) Song, X. Y.; Zhang, Y. H.; Sun, P. P.; et al. Lithium−lanthanide bimetallic metal−organic frameworks towards negative electrode materials for lithium-ion batteries. *Chem.—Eur. J.* **2020**, *26*, 5654−5661.
(13) Phan, A.; Doonan, C. J.; Uribe-Romo, F. J.; et al. Synthesis, structure, and carbon dioxide capture properties of zeolitic imidazolate frameworks. *Acc. Chem. Res.* **2010**, *43*, 58−67.
(14) Karagiaridi, O.; Lalonde, M. B.; Bury, W.; Sarjeant, A. A.; Farha, O. K.; Hupp, J. T. Opening ZIF-8: a catalytically active zeolitic imidazolate framework of sodalite topology with unsubstituted linkers. *J. Am. Chem. Soc.* **2012**, *134*, 18790−18796.
(15) Banerjee, R.; Phan, A.; Wang, B.; et al. High-throughput synthesis of zeolitic imidazolate frameworks and application to $CO_2$ capture. *Science* **2008**, *319*, 939−943.
(16) Noh, K.; Lee, J.; Kim, J. Compositions and structures of zeolitic imidazolate frameworks. *Isr. J. Chem.* **2018**, *58*, 1075−1088.
(17) Tan, Y. X.; Wang, F.; Zhang, J. Design and synthesis of multifunctional metal-organic zeolites. *Chem. Soc. Rev.* **2018**, *47*, 2130−2144.
(18) Pimentel, B. R.; Parulkar, A.; Zhou, E.; et al. Zeolitic imidazolate frameworks: next-generation materials for energy-efficient gas separations. *ChemSusChem* **2014**, *7*, 3202−3240.
(19) Zheng, Z.; Rong, Z.; Nguyen, H. L.; et al. Structural chemistry of zeolitic imidazolate frameworks. *Inorg. Chem.* **2023**, *62*, 20861−20873.
(20) Yang, J. J.; Zhang, Y. B.; Qi, L.; et al. Principles of designing extra-large pore openings and cages in zeolitic imidazolate frameworks. *J. Am. Chem. Soc.* **2017**, *139*, 6448−6455.
(21) Nguyen, N. T. T.; Furukawa, H.; Gándara, F.; et al. Selective capture of carbon dioxide under humid conditions by hydrophobic chabazite-type zeolitic imidazolate frameworks. *Angew. Chem., Int. Ed.* **2014**, *53*, 10645−10648.
(22) Hayashi, H.; Côté, A. P.; Furukawa, H.; et al. Zeolite A imidazolate frameworks. *Nature materials* **2007**, *6*, 501−506.
(23) Shi, Q.; Xu, W. J.; Huang, R. K.; et al. Zeolite CAN and AFI-type zeolitic imidazolate frameworks with large 12-membered ring pore openings synthesized using bulky amides as structure-directing agents. *J. Am. Chem. Soc.* **2016**, *138*, 16232−16235.
(24) Meng, Q.; Wang, J.; Shi, Q.; et al. Synthesis of a new ATN-type zeolitic imidazolate framework through cooperative effects of N,N-dipropylformamide and n-butylamine. *CrystEngComm* **2021**, *23*, 3429−3433.
(25) Park, K. S.; Ni, Z.; Côté, A. P.; et al. Exceptional chemical and thermal stability of zeolitic imidazolate frameworks. *Proc. Natl. Acad. Sci. U. S. A.* **2006**, *103*, 10186−10191.
(26) Tian, Y. Q.; Zhao, Y. M.; Chen, Z. X.; et al. Design and generation of extended zeolitic metal-organic frameworks (ZMOFs): Synthesis and crystal structures of zinc(II) imidazolate polymers with zeolitic topologies. *Chem.—Eur. J.* **2007**, *13*, 4146−4154.
(27) Ramirez, J. R.; Yang, H.; Kane, C. M.; et al. Reproducible synthesis and high porosity of mer-$Zn(Im)_2$ (ZIF-10): Exploitation of an apparent double-eight ring template. *J. Am. Chem. Soc.* **2016**, *138*, 12017−12020.
(28) Brekalo, I.; Kane, C. M.; Ley, A. N.; et al. Use of a ″shoe-last″ solid-state template in the mechanochemical synthesis of high-porosity RHO-zinc imidazolate. *J. Am. Chem. Soc.* **2018**, *140*, 10104−10108.
(29) Tian, Y. Q.; Cai, C. X.; Ren, X. M.; et al. The silica-like extended polymorphism of Cobalt(II) imidazolate three-dimensional frameworks: X-ray single-crystal structures and magnetic properties. *Chem.—Eur. J.* **2003**, *9*, 5673−5685.
(30) Schröder, C. A.; Baburin, I. A.; Van Wüllen, L.; et al. Subtle polymorphism of zinc imidazolate frameworks: Temperature-dependent ground states in the energy landscape revealed by experiment and theory. *CrystEngComm* **2013**, *15*, 4036−4040.
(31) Shi, Q.; Kang, X.; Shi, F. N.; et al. $Zn_{10}(Im)_{20}$·4DBF: an unprecedented 10-nodal zeolitic topology with a 10-MR channel and 10 crystallographically independent Zn atoms. *Chem. Commun.* **2015**, *51*, 1131−1134.
(32) Lehnert, R.; Seel, F. Preparation and crystal structure of the manganese (II) and zinc (II) derivative of imidazole. *Z. Anorg. Allg. Chem.* **1980**, *464*, 187.
(33) Guo, S.; Li, H. Z.; Wang, Z. W.; et al. Syntheses of new zeolitic imidazolate frameworks in dimethyl sulfoxide. *Inorganic Chemistry Frontiers* **2022**, *9*, 2011−2015.
(34) Lawton, S. L.; Rohrbaugh, W. J. The framework topology of ZSM-18, a novel zeolite containing rings of three (Si,Al)-O species. *Science* **1990**, *247*, 1319−1322.
(35) Hu, M. L.; Masoomi, M. Y.; Morsali, A. Template strategies with MOFs. *Coord. Chem. Rev.* **2019**, *387*, 415−435.
(36) Sheldrick, G. M. *SHELXS-97, Program for Crystal Structure Solution*; University of Göttingen: Germany, 1997.
(37) Sheldrick, G. M. *SHELXL-97, Program for Crystal Structure Refinement*; University of Göttingen: Germany, 1997.
(38) Ma, Y.; Hu, J.; Fan, K.; et al. Design of an organic template for synthesizing ITR zeolites under Ge-free conditions. *J. Am. Chem. Soc.* **2023**, *145*, 17284−17291.
(39) Gao, M.; Wang, J.; Rong, Z.; et al. A combined experimental-computational investigation on water adsorption in various ZIFs with the SOD and RHO topologies. *RSC Adv.* **2018**, *8*, 39627−39634.
(40) Gao, M.; Huang, R. K.; Zheng, B.; et al. Large breathing effect in ZIF-65(Zn) with expansion and contraction of the SOD cage. *Nat. Commun.* **2022**, *13*, 4569.
(41) He, C.; Li, S.; Xiao, Y.; et al. Application of solid-state NMR techniques for structural characterization of metal-organic frameworks. *Solid State Nucl. Magn. Reson.* **2022**, *117*, No. 101772.


https://doi.org/10.1021/acsomega.4c04259
*ACS Omega* 2024, 9, 34777−34786

(42) Chang, X. W.; Yan, W. F.; Shi, W.; et al. Influence of environment change around N-atom on the structure-directing effect of methylamine in the synthesis of open-framework aluminophosphates. *Chemical Journal of Chinese Universities* **2018**, *39*, 12−18.



https://doi.org/10.1021/acsomega.4c04259
*ACS Omega* 2024, 9, 34777−34786